

---

# A NEW MODEL FOR THE ORIGIN OF PYROCHLORE: EVIDENCE FROM THE ST HONORÉ CARBONATITE, CANADA

O.V. Vasyukova and A.E. Williams-Jones

*Department of Earth and Planetary Sciences, McGill University, 3450 University Street Montréal,  
Québec, Canada, H3A 0E8*

## Abstract

The Neoproterozoic St Honoré carbonatite complex is one of three currently mined niobium deposits. In these and most other carbonatite-hosted niobium deposits, pyrochlore is the principal ore mineral. Four major pyrochlore-bearing rock types are observed in the St Honoré complex, namely, biotitite, magnetite-biotite rock, apatitite and carbonatite. The textural relationships among the different rock types and within each rock type are extremely complex, as are the textures and crystal chemistry of the pyrochlore. Compositionally, there are two major types of pyrochlore. Type-1 is enriched in Ta, U, Zr, Sr, Th, Fe, REE and Cl and Type-2 is a Ca-Na-F-rich pyrochlore, with proportions of other elements close to or below their detection limits. Type-1 pyrochlore is yellow- to red-brown and, in many cases, displays oscillatory zoning. This variety occurs most commonly in the cores of crystals in apatitite, where it has its highest concentrations of the elements listed above. It also is observed in biotitite, but the proportions of the above elements are much lower. Type-2 pyrochlore is light to dark brown and, generally, does not exhibit oscillatory zoning. It forms overgrowths on Type-1 pyrochlore in apatitite and biotitite, and occurs as large crystals in the magnetite-biotite rock (Type-1 pyrochlore is not present in magnetite-biotite rock). We propose that Type-1 pyrochlore crystallised from a highly evolved, fluid-undersaturated carbonatitic magma, whereas Type-2 pyrochlore crystallised from a carbonatitic magma that had undergone fluid exsolution, which depleted the magma in elements that tend to partition preferentially into aqueous fluids, i.e., U, Sr, Fe, REE, Ba and Cl.

The processes that governed the evolution of the carbonatitic magma (which was mantle-derived and introduced in numerous small batches) and crystallisation of pyrochlore at St Honoré were biotitisation (by the magma), crystallisation of calcite and aqueous fluid exsolution. Biotitisation

of the host syenite consumed MgO, H<sub>2</sub>O and CO<sub>2</sub> from each magma batch (the CO<sub>2</sub> was released as a gas), leading to the crystallisation of Type-1 pyrochlore in biotite. This process also locally increased the CaO content of the magma to a level sufficient to saturate it with calcite leaving a residual phoscoritic magma that crystallised the most Ta-U-enriched variety of Type-1 pyrochlore. Exsolution of the aqueous fluid occurred as a result of prolonged crystallisation and/or pressure release and led to the crystallisation of Type-2 pyrochlore. The evolution of each of the magma batches was different and depended on the extent of biotitisation, on whether calcite crystallised, and on the timing of fluid exsolution. As the two types of pyrochlore and their temporal relationship have been described for many carbonatite complexes, the hypotheses presented in this paper are likely also applicable to the genesis of pyrochlore in these other complexes.

## Introduction

Niobium is an essential component in many high technology applications (mostly as a component of high-strength, corrosion-resistant, low-alloy steels and superalloys) and is considered a critical metal because of its economic importance and high supply risk. The main sources for niobium are carbonatite complexes and their weathered products (laterites), in which pyrochlore is the main ore mineral.

Many studies of pyrochlore have discussed its crystal chemistry, structure (e.g., sector and oscillatory zoning), classification and nomenclature (Hogarth et al., 2000; Chakhmouradian and Williams, 2004; Zurevinski and Mitchell, 2004; Lee et al., 2006; Chakhmouradian et al., 2015; Mitchell, 2015; Guarino et al., 2017; Walter et al., 2018; Mitchell et al., 2020; da Costa et al., 2021; Dey et al., 2021; Zaitsev et al., 2021). Studies that focus on its origin have reached the conclusion that the magma crystallising the pyrochlore-hosting carbonatite was not the parental magma for the pyrochlore, i.e., the observed pyrochlore is of xenocrystic or antecrystic origin. For example, Zurevinski and Mitchell (2004), noting that two or more varieties of pyrochlore commonly occur in close proximity to each other in the Oka carbonatite, concluded that none of these pyrochlore varieties crystallised in-situ, and instead, crystallised elsewhere from separate batches of carbonatitic magma that mixed and transported the pyrochlore to its current location. Mitchell (2015), in a review of carbonatite-hosted niobium deposits, proposed that the pyrochlore observed in carbonatites crystallises as an early liquidus mineral from a carbonated silicate magma, which subsequently evolves to a carbonatitic magma. According to this hypothesis, the pyrochlore

accumulates on the walls and the floor of the magma chamber hosting the silicate liquid and is subsequently eroded by and incorporated in the late evolving carbonatitic magma. More recently, Mitchell et al. (2020), in a study of the Good Hope carbonatite, proposed that the pyrochlore, which is concentrated in apatite segregations, crystallised as the first liquidus mineral from an “unidentified” carbonatitic magma and mixed with a second “unidentified” carbonatitic magma, in which apatite was the first liquidus mineral, producing the apatite-pyrochlore segregations that were subsequently transported as clasts in a third magma.

A major reason for the complex ex-situ (xenocrystic) models that have been proposed is the considerable compositional and textural heterogeneity of carbonatite-hosted pyrochlore. In this paper, we propose an in-situ model that avoids the need to invoke unidentified magma sources and magma chambers and satisfactorily explains the commonly observed pyrochlore heterogeneity. The model is based on observations made for the St Honoré carbonatite and a hypothesis presented in Vasyukova and Williams-Jones (2022) and tested in Vasyukova et al. (2023), in which a reaction of the carbonatitic magmas with their host rocks and consumption of the major carbonate oxides (CaO, MgO and H<sub>2</sub>O) provides an additional means of magma evolution. Instead of attributing the pyrochlore heterogeneity to its ex-situ crystallisation, this model relates the heterogeneity to its in-situ crystallisation from a mantle-derived carbonatitic magma that evolved through variable degrees of magma-rock interaction, calcite crystallisation and fluid exsolution (see also Williams-Jones and Vasyukova, 2022). We believe that this model identifies the major factors controlling the concentration of niobium to economic levels in carbonatites and by so doing also significantly advances our understanding of the genesis of carbonatite complexes.

## Geological setting

The St Honoré alkaline complex (Québec, Canada), which is roughly elliptical in plan (4 x 5 km), was emplaced at  $571 \pm 5$  Ma (McCausland et al., 2009) in rocks of the ~1 Ga Grenville Metamorphic Province, and comprises an outer domain of alkaline syenites and lesser nepheline-cancrinite-garnet-bearing syenites and an inner domain of carbonatites (Thivierge et al., 1983). The carbonatite domain consists of an exterior zone of calcite-rich carbonatites, an interior zone of dolomite-rich carbonatites and a rare earth element (REE)-rich ferro-carbonatite core (Fig. 1). Each zone comprises numerous individual intrusions of carbonatite varying in thickness from a few centimetres to several metres (rare). Our study focused on the south-west part of the complex

(calcite-rich and dolomite-rich carbonatites), which contains a niobium resource of 416 Mt grading 0.42 wt% Nb<sub>2</sub>O<sub>5</sub> that has been mined since 1976 (Vallieres et al., 2013). Significantly, this relatively minor part (500 x 800 m) of the complex is centred on a small body of variably fragmented syenite (Fig. 1) that has been biotitised to varying degrees; in the extreme, the rock is a fine-grained biotitite (glimmerite). Calcite-rich carbonatites are concentrated proximal to biotitised syenite. In addition to the carbonatites and variably biotitised syenite, coarse-grained magnetite-biotitite rock and apatitite are also observed. The apatitite occurs as layers and lenses in both varieties of carbonatite, but more commonly in the dolomite carbonatite, whereas the magnetite-biotite rock is concentrated near the contact between biotitite and carbonatite (this unit is interpreted to be a cumulate). The relationships among the different units are extremely complex involving numerous intrusions of carbonatite (with both sharp and gradational contacts) and multiple alteration episodes.

## **Rock types**

The syenite (alkaline syenite) consists dominantly of early perthite, later albite and K-feldspar and, as mentioned above, has been variably biotitised. The biotitisation was the result of the replacement of the K-feldspar and perthite by biotite and was most intense where the fragmentation of the syenite was most advanced (almost invariably, cm-sized fragments of syenite in the carbonatite have been completely replaced by biotite). Figure 2a illustrates incipient biotitisation and Figure 2b extreme biotitisation. With increasing distance from unaltered syenite, the proportion of biotite (fine-grained) increases progressively to form the biotitite that, in places, reaches tens of metres in thickness. Commonly, but not exclusively, the biotitite passes into the magnetite-biotite rock or directly into carbonatite that frequently contains apatite-rich layers and lenses. Pyrochlore is present in all of these units and is described in detail below.

Samples of the biotitite commonly contain up to 70 vol % of fine-grained (5-15 µm) biotite, although some larger biotite crystals (up to 300 µm) may also be present. Magnetite is the next most abundant mineral and occurs mainly as small (5-50 µm) anhedral crystals that post-dated the fine-grained biotite; there are also larger crystals (up to 200-300 µm), typically in association with interstitial calcite or, more commonly, dolomite. Some samples of the biotitite contain abundant tiny zircon crystals (5-15 µm) that, in some cases, form aggregates.

The magnetite-biotite rock, as noted above, commonly occurs in close spatial association with biotite in a zone between the latter and carbonatite. This rock unit comprises variable proportions of large biotite and magnetite crystals in a matrix of subordinate dolomite (Figs. 2c and d). The biotite and magnetite crystals are typically euhedral and vary in size on a cm scale (individual crystals range from less than a mm to several cm in diameter; Fig. 2d). In rare cases, apatite is observed as inclusions in magnetite and as small aggregates around magnetite. These textural relationships indicate that biotite and magnetite crystallised at roughly the same time, that they were preceded by apatite and were post-dated by dolomite.

The apatite is represented by fluorapatite-rich aggregates (hereafter, apatite refers to fluorapatite) containing subordinate proportions of biotite, magnetite (Fig. 2e) and minor zircon, and is observed in both calcite and dolomite carbonatite. All the minerals are euhedral to subhedral, and their crystals are variable in size. Apatite crystals vary from 150 to 400  $\mu\text{m}$  and 20 to 100  $\mu\text{m}$  in length and width, respectively. The biotite and magnetite crystals are larger, 0.2-2 mm and 0.1-1 mm in diameter, respectively, and the zircon crystals are somewhat smaller, up to 0.5 mm in diameter (the zircon contains numerous inclusions of apatite). Textural relationships indicate that biotite was the earliest mineral to crystallise followed by apatite, magnetite and zircon, which crystallised pene-contemporaneously.

As mentioned above, the Nb mineralisation is associated with both calcite and dolomite carbonatites. The early carbonatites are either homogeneous (pink or grey depending on whether they are altered) or contain layers/lenses of apatite (banded). In most cases, they contain a single carbonate mineral, either calcite or dolomite (in very rare cases, both minerals may be found in the same sample), and, where the carbonate mineral is dolomite, several generations may be manifested by differences in grain size and the occurrence of small dolomite crystals as inclusions in larger dolomite crystals. In contrast, the late carbonatites, which do not contain apatites except as rare fragments, are invariably dolomitic and homogeneous. Where contacts between the different carbonatite intrusions are preserved, they are delineated either by a difference in the colour of the two carbonatites or by crosscutting relationships in which the layering of the early carbonatite is terminated by the later carbonatite (Fig. 2f).

## **Analytical methods**

The study was based on a suite of 20 samples from the mine workings and 87 samples from drill core, from which 32 samples were selected for detailed petrographic examination and quantitative microanalysis of the pyrochlore. The petrographic examination was conducted with an optical microscope and a Hitachi SU5000 field emission scanning electron microscope (SEM) equipped with an Oxford Instruments X-Max<sup>N</sup> 80 silicon drift detector to provide semi-quantitative analyses. Pyrochlore compositions were determined quantitatively using a Cameca SX 100 FIVE FE electron microprobe equipped with five wavelength-dispersive spectrometers and an Si(Li) energy-dispersive spectrometer. The analyses (5 µm beam diameter) were conducted at 20 kV with a 20 nA beam current.

## The nature and distribution of pyrochlore

Pyrochlore has the generalized formula  $A_{2-m}B_2X_{6-w}Y_{1-n}$ , where m, w and n refer to vacancies (Atencio et al., 2010). At St Honoré, the main A-site elements are Ca, Na, Fe, U, Sr, Th and the REE and the main B-site elements are Nb, Ti, Si, Ta and Zr. Fluorine and OH are the main occupants of the Y-site. The texture and mode of occurrence of the pyrochlore differs considerably within and among the different rock units described above. Compositionally, however, most of the pyrochlore classifies as calciopyrochlore (Fig. 3). A small proportion of pyrochlore hosted by apatite has a large enough proportion of A-site vacancies to classify it as kenopyrochlore (Fig. 3). Below, we describe the nature and composition of the pyrochlore according to its host. A full set of compositional data for pyrochlore from the different units is reported in Table A1 in Supplementary material.

## Biotite

Pyrochlore in the biotite forms tiny euhedral brown crystals (typically 5-50 µm in diameter, 150 µm in diameter in the extreme). They occur either as inclusions in biotite (which, in some cases, altered to chlorite) or as crystal aggregates between biotite crystals (Fig. 4a) and, in strongly biotitised syenite, they are surrounded, partly or wholly, by magnetite (Figs. 4b and c). In many cases, the aggregates define the boundary between fine-grained and coarse-grained biotite (Fig. 4d). The magnetite-associated pyrochlore crystals are larger and lighter in colour than those associated with biotite. They also contain inclusions of biotite, showing that this pyrochlore post-dates the biotite-associated pyrochlore (Fig. 4c). Optically, the latter appears unaltered, whereas

the pyrochlore associated with magnetite contains colourless patches (alteration). Zircon crystals are present in some of the pyrochlore aggregates and also occurs as inclusions in biotite. Commonly, biotite crystals hosting or adjacent to pyrochlore display radiation damage (Figs. 4a-c). Rare samples of biotitised syenite contain apatite aggregates with subordinate pyrochlore. In backscattered electron (BSE) images, the biotite- and magnetite-associated pyrochlore contains a bright core (in many cases with brighter vermicules, which are interpreted to be the result of alteration) and a darker rim (Fig. 4f). In contrast, the pyrochlore of the apatite aggregates is homogeneously dark.

The pyrochlore cores are enriched in U and Ta, and are somewhat depleted in Ca, F and Na compared to the pyrochlore rims (Figs. 5a and b, Table 1 and Table A1). They also contain appreciable REE (up to 1.5 wt.% total REE) and have a significant A-site deficiency (Fig. 5b); Th and Zr are at and below the detection limit, respectively (Table 1). The F content of the pyrochlore cores ranges from 2 to 4 wt.%. The brighter pyrochlore (in BSE images; vermicular/altered) is compositionally identical to the pyrochlore core except for a higher content of Fe (up to 2.3 wt.% FeO; Table A1). In addition to Nb, the pyrochlore cores also contain small proportions of Ti, Si and Fe in the B-site (Fig. 5c). In contrast to the pyrochlore cores, the pyrochlore rims have very low concentrations of U and Ta (Figs. 5a and c). They also have very few A-site vacancies (Fig. 5b) and a high, effectively constant, F content (4-4.3 wt.%; Table 1). In summary, the pyrochlore cores are represented by a non-stoichiometric pyrochlore with a significant proportion of A-site vacancies and elevated proportions of cations other than  $\text{Ca}^{2+}$ ,  $\text{Na}^{+}$  and  $\text{Nb}^{5+}$  and  $\text{OH}^{-}$ , whereas the pyrochlore rims have a composition of nearly stoichiometric fluorcalciopyrochlore.

## **Magnetite-biotite rock**

The pyrochlore crystals in the magnetite-biotite rock are large (250-500  $\mu\text{m}$  on average), euhedral and light to dark brown (Fig. 6), in rare cases displaying fine oscillatory zoning, in which the layers are alternately brown and light brown to colourless. The intensity of the brown colour is determined by the proportion of nano-inclusions of a dark, needle-like mineral (ilmenorutile?). Most pyrochlore crystals display patchy colourless alteration associated with crystals of baddeleyite and columbite-(Fe) (Figs. 6c and d). Textural relationships show that the pyrochlore began crystallising late relative to the biotite (small crystals of pyrochlore are included in the rims of biotite), but coincident with the crystallisation of magnetite (magnetite contains inclusions of

pyrochlore and pyrochlore contains inclusions of magnetite). Unlike the pyrochlore in the biotitite, which comprises bright and dark varieties in BSE images, there is only one, homogeneous variety in BSE images in the magnetite-biotite rock.

Chemically, the pyrochlore is similar to the dark (in BSE images) pyrochlore in the biotitite in that the U and Ta contents are below detection and close to detection, respectively, and it has a nearly stoichiometric composition with very low proportion of A-site vacancies (Figs. 5a and b, Table 1 and Table A1). This pyrochlore differs from the pyrochlore in the biotitite, however, by having elevated contents of Zr, Th and Ti (Fig. 5c; Table 1), except where altered. Where it is altered, the Zr content is near the detection limit, which likely explains the association of the alteration with baddeleyite.

## **Apatitite**

As noted earlier, apatitite occurs in both the calcite carbonatite and the dolomite carbonatite, but is more common in the latter. Although the textures of pyrochlore in the apatitite are very complex, the only difference between pyrochlore in apatitite hosted by calcite carbonatite and pyrochlore in apatitite hosted by dolomite carbonatite is that the crystals in the former tend to be smaller and more euhedral than in the dolomite carbonatite (Figs. 7a and b). Optically, the pyrochlore can be subdivided into a darker core and a lighter-coloured rim. In most cases, the core underwent resorption before being overgrown by the rim (Figs. 7c and d), although in some rare cases, the rims are overgrown on euhedral cores. Commonly, the cores show evidence of strong alteration, which destroyed any primary zonation that may have been present (Fig. 7c), but in cases where the alteration was weaker, up to three zones may be observed (Fig. 7d). The first of these zones is optically colourless, the second is yellow to red-brown and homogeneous and the third is darker with oscillatory zoning (zones 1, 2 and 3 in Figure 7d, respectively). In BSE images, Zone 1 is dark and Zone 2 is bright. By contrast, Zone 3 alternates between dark and bright, suggesting that it may record the crystallisation of the pyrochlore types in Zone 1 and Zone 2.

The overgrowth and, in some samples, Zone 3, contains numerous inclusions of apatite, some of which host solid-bearing H<sub>2</sub>O-CO<sub>2</sub> fluid inclusions with variable phase ratios (Fig. 7e). More importantly, the apatite cores, which most likely crystallised at the same time as apatite included in the overgrowths, also are rich in solid-bearing H<sub>2</sub>O-CO<sub>2</sub> fluid inclusions with variable phase



ratios; barite and burbankite  $\{(\text{Na,Ca})_3(\text{Sr,Ba,Ce})_3(\text{CO}_3)_5\}$  are the most common solids. Less commonly, the overgrowths contain inclusions of magnetite. Where the pyrochlore displays oscillatory zoning, the intensity of the colour is determined by the proportion of nano-inclusions of a needle-like mineral (ilmenorutile?). As noted above, the cores commonly display evidence of strong alteration. This is manifested by the destruction of primary textures and the occurrence of baddeleyite. The overgrowths also have been strongly altered, as shown by the occurrence of colourless patches superimposed upon the oscillatory zoning and radial fractures with light-coloured haloes (Fig. 7d). Commonly, the colourless patches contain small irregularly shaped crystals of columbite-(Fe) and baddeleyite. Pyrochlore close to the contact between early (banded) and late (homogeneous) carbonatites has been partially or completely replaced by columbite-(Fe).

The pyrochlore cores hosted by apatite display a wide range of compositions and reach the highest contents of U, Ta, Ti, Zr, Si and the maximum proportions of A-site vacancies as well as the lowest concentrations of Ca, Na and F of any studied pyrochlore (Fig. 5). Other elements that occur in the highest concentrations in this pyrochlore are Fe, Sr, REE and Th (Table 1). Moreover, only this pyrochlore contains Cl and significant Ba and Si (Table A1).

As mentioned above, the cores of the unaltered pyrochlore comprise two varieties in BSE images, one corresponding to Zone 1 (dark) and the other to Zone 2 (bright), with Zone 3 representing an alternation (oscillatory zoning) of the two varieties. In Ta-U-Ca+Na coordinates, the first variety (Zone 1) forms a trend with a constant Ta/U ratio and varying proportions of the Ca+Na component, whereas the second variety lies on a line of constant (and very high) Ta content with varying proportions of U and Ca+Na (Fig. 8). As expected from the alternation of dark and bright layers in Zone 3, the composition of Zone 3 pyrochlore plots on both trends.

The overgrowths (dark in BSE images) have a composition very close to that of fluorcalciopyrochlore (Fig. 5). The only additional components in significant proportions are Ti, Zr and Th. Compositionally, the overgrowths are remarkably similar to pyrochlore in the magnetite-biotite rock, in that even the proportions of Ti, Zr and Th are statistically indistinguishable (Table 1). The pyrochlore cores in the biotite are also compositionally similar, but have lower concentrations of Ti, Zr and Th (Fig. 5c).

As noted above, both the overgrowths and the cores display evidence of alteration. Compositionally, the altered pyrochlore in the overgrowths (colourless patches) is indistinguishable from that of the unaltered overgrowth, except for a much lower concentration of Zr (Table 1A). In contrast, the altered pyrochlore in the core has a composition intermediate between that of the overgrowths and Zones 2 and 3 of the unaltered core.

## **Carbonatite**

Although much of the pyrochlore is hosted by the rock types described above, some pyrochlore is hosted by the carbonate fraction of the banded carbonatite and the late dolomite carbonatite (Fig. 9). Most of the pyrochlore in these units occurs in small fragments of biotitite or apatitite. Locally, the apatitite fragments have partially disaggregated as a result of the dissolution of the apatite (Fig. 9). In rare cases (mainly in the late carbonatite), the pyrochlore occurs as discrete euhedral crystals between carbonate crystals and as inclusions in carbonate minerals. Compositionally, the pyrochlore is highly variable and includes the full range of compositions reported for the other rock types (Fig. 5, Table 1 and Table A1).

## **Discussion**

### **Compositional types of pyrochlore**

As is evident from the preceding descriptions, the pyrochlore in the St Honoré carbonatite can be subdivided into two types. Type-1 pyrochlore (cores in apatitite and biotitite) is Ta-U-rich and is also enriched in Sr, Fe, REE, Th and Zr (and in the apatitite, in Ba, Si and Cl). This pyrochlore is characterised by considerable compositional heterogeneity both within a single sample and among samples, a high proportion of A-site vacancies and low contents of F, Ca and Na (Fig. 5). In contrast, the Type-2 variety (overgrowths in apatitite and biotitite and pyrochlore from magnetite-biotite rock) has a nearly ideal stoichiometric composition, i.e., a high content of Ca, Na and F, very few A-site vacancies and low or undetectable concentrations of Ta, U, Sr, Ba, Fe, Si, Th, Zr and Cl. An exception to this is the Type-2 pyrochlore in the magnetite-biotite rock and pyrochlore overgrowths in apatitite, which is commonly enriched in Th and Zr. The occurrence of these two compositional types of pyrochlore and the heterogeneity of the first type is not restricted to St Honoré. Indeed, it is a feature of almost every carbonatite, for which information on pyrochlore compositions has been published, e.g., a number of carbonatites in the Kola Peninsula, Russia

(Chakhmouradian et al., 2004), the Aley carbonatite, Canada (Chakhmouradian et al., 2015), the Sokli carbonatite, Finland (Lee et al., 2006), the Kaiserstuhl carbonatite, Germany (Walter et al., 2018), the Bailundo carbonatite, Angola (da Costa et al., 2021) and the Catalão I and II carbonatites (Guarino et al., 2017). The absolute concentrations of Ta, U and the other elements, in the two types of pyrochlore, however, differs considerably among the different carbonatites.

Most researchers have concluded that the two pyrochlore types are either antecrystic or xenocrystic and have not attempted to interpret the controls on their composition. To our knowledge, only Chakhmouradian and Williams (2004) and Chakhmouradian et al. (2015) have tackled this issue. Both attributed the enrichment of Ta in Type-1 pyrochlore to a greater availability of Ta during the early stages of carbonatitic magma evolution. The textural relationships involving pyrochlore at St Honoré clearly indicate that Type-1 pyrochlore crystallised earlier than Type-2 pyrochlore, consistent with the explanation of Chakhmouradian and Williams (2004) and Chakhmouradian et al. (2015). However, this explanation cannot account for the enrichment in elements other than Ta, such as U, Sr, Fe, REE, Ba and Cl. In the case of the Aley carbonatite, Chakhmouradian et al. (2015) concluded that fluorcalciopyrochlore (Type-2) formed because F-bearing silicate minerals, such as biotite and amphibole, ceased to crystallise. Although F-rich biotite stopped crystallising before the crystallisation of pyrochlore Type-2 at St Honoré, this was not accompanied by the crystallisation of non-F-bearing minerals. Consequently, the increase in the activity of F in the magma necessary to saturate it with F-rich pyrochlore did not occur.

Below, we propose an alternative model for the crystallisation of Type-1 and Type-2 pyrochlore at St Honoré. In so doing, we also address the broader question of how a carbonatitic magma might saturate with pyrochlore and why the processes that explain this saturation inevitably lead to an evolution of the magmas that is punctuated by the crystallisation of two distinctly different pyrochlore types.

## **A model for pyrochlore crystallisation**

The evolution of the early (Type-1) pyrochlore at St Honoré is best exemplified by the pyrochlore hosted in apatite. As discussed above, this pyrochlore comprises three zones, a colourless but relatively homogeneous core (Type-1a), a darker homogeneous yellow to red-brown mantle (Type-1b) and a rim that is characterised by an oscillation of fine layers of Type-1a and Type-1b

pyrochlore. Both varieties are enriched in Ta, U, Zr, Sr, Th, Fe, REE and Cl, although to a different extent (Type-1b is more enriched). There are two prerequisites for the enrichment of these elements in the Type-1 pyrochlore, 1) the magma should contain elevated concentrations of these elements and 2) the pyrochlore/magma partition coefficients should favour their incorporation into the pyrochlore. The high concentrations of incompatible elements like U, Ta, Th and Zr in the magma requires that it must have been highly evolved, which is also consistent with the ability of this magma to saturate in pyrochlore, a mineral that is extremely soluble in carbonatitic liquids (Jago and Gittins, 1993; Mitchell and Kjarsgaard, 2002; Mitchell and Kjarsgaard, 2004).

A striking feature of the Type-1 pyrochlore is the alternation of Type-1a and Type-1b varieties. According to Hogarth et al. (2000), a change in temperature-pressure conditions, magma mixing or delays in crystal growth should only produce a relatively simple pattern of growth and cannot explain the complex oscillatory zonation observed in some pyrochlore crystals. They concluded that an undisturbed environment and alternating supersaturation in two end-members of the crystallising mineral are the principal causes of oscillatory zoning. We, therefore, propose that the early pyrochlore at St Honoré, Type-1a, formed under relatively quiescent conditions as a result of the supersaturation of the magma with the respect to this phase (a more stable, closer to end-member variety) and continued to grow (Zone 1) until it was replaced by a second variety, Type-1b. This variety was much more enriched in Ta, U, Zr and other incompatible elements and saturated in the magma to form Zone 2. The latter occurred because of the build-up of Ta, U and other elements in a boundary layer magma and the decrease in the degree of supersaturation of Type-1a pyrochlore due to its crystallisation. The oscillatory zoned pyrochlore (Zone 3) is interpreted to represent the alternate crystallisation of Type-1a and Type-1b pyrochlore as elaborated above, i.e., Type-1a layers were replaced by Type-1b layers when the level of supersaturation of the Type-1b pyrochlore in the boundary layer magma exceeded that of the Type-1a pyrochlore. We propose that the fine scale of this zoning reflects the evolution of the residual magma to higher viscosity, which inhibited diffusion of components to and from the crystallising surface and promoted the development and consumption of a narrow boundary layer.

As mentioned earlier, there was an abrupt compositional change from Type-1 to Type-2 pyrochlore in apatite. Whereas Type-1 pyrochlore is enriched in U, Ta and a number of other elements (see above), Type-2 pyrochlore is generally characterised by a near end-member stoichiometric

composition (fluorcalciopyrochlore). Significantly, many of the elements, in which the Type-2 pyrochlore is depleted, are typically fluid-mobile (U, Sr, Ba,  $\text{Fe}^{2+}$ , REE and Cl). Moreover, as mentioned earlier, apatite inclusions in Type-2 pyrochlore and coexisting apatite cores, both contain solid-bearing  $\text{H}_2\text{O}-\text{CO}_2$  fluid inclusions, and the most common solids are barite and burbankite, i.e., minerals enriched in the fluid-mobile elements, Ba, Sr, and the REE. We propose that the fluid inclusions in apatite record the exsolution of a magmatic-hydrothermal fluid and that this exsolution caused the transition from Type-1 to Type-2 pyrochlore by changing the magma composition through the release of the above fluid-mobile elements. We also propose that the element release was promoted by the acidic nature of the fluid because of the saturation of the latter with  $\text{CO}_2$ . This left Na and Ca as the only elements that could occupy the A-site of the subsequently crystallising Type-2 pyrochlore. As the hydroxide ion was lost to the fluid, the F/OH ratio in the residual magma increased sharply and, as a result, the Y-site of the Type-2 pyrochlore is dominated by F. Because of the tendency of Ta to avoid fluorine in pyrochlore (Kjarsgaard and Mitchell, 2008), this also explains the low content of Ta in Type-2 pyrochlore. In addition, the strong increase in F activity likely triggered crystallisation of fluorapatite, consistent with the observation that apatite and Type-2 pyrochlore crystallised at the same time. Finally, the exsolution of fluid increased the concentration of the fluid-immobile elements (e.g., Zr, Th and  $\text{Fe}^{3+}$ ) in the residual magma. This increase in concentration, in turn, led to the saturation of the magma in Th-bearing zircon and magnetite.

As discussed earlier, both the apatite and biotite contain Type-1 and Type-2 pyrochlore. The mode of occurrence of the Type-1 pyrochlore in the biotite, however, differs from that in the apatite (it is zoned in the apatite and unzoned in the biotite). Compositionally, the Type-1 pyrochlore in the biotite is similar to the Type-1a pyrochlore in the apatite, i.e., it has relatively low (for Type-1 pyrochlore) contents of U and Ta, reflecting a less evolved magma than the magma that crystallised the Type-1b pyrochlore in the apatite. The absence of oscillatory zoning in the biotite-hosted Type-1 pyrochlore points to a more turbulent and lower viscosity magma than was the case for the magma that crystallised Type-1 pyrochlore in the apatite. The Type-2 pyrochlore in the biotite is compositionally very similar to the Type-2 pyrochlore in the apatite and only differs from the latter in having much lower Zr and Th contents. We consider that Type-2 pyrochlore in the biotite, like that in the apatite, crystallised in response to the exsolution of a magmatic hydrothermal fluid that removed the fluid-mobile elements (U, Sr, Ba,  $\text{Fe}^{2+}$ , REE and

Cl) promoting the crystallisation of stoichiometric fluorcalciopyrochlore; the high proportion of F reflects the loss of OH to the fluid (see above). The unusually low concentrations of Zr and Th in both Type-1 and Type-2 pyrochlore in biotitite are attributed to the large scale crystallisation of zircon in response to the high activity of Si that accompanied formation of the biotitite (see below).

Unlike the pyrochlore hosted by apatitite and biotitite, the pyrochlore of the magnetite-biotite rock is exclusively the Type-2 variety. This pyrochlore is compositionally very similar to the Type-2 pyrochlore in the apatitite. The probable reason for the absence of Type-1 pyrochlore is that the magnetite-biotite rock only crystallised after the exsolution of the magmatic hydrothermal fluid. This explanation is consistent with the abundance of magnetite, which we attribute to the elevated concentration of  $\text{Fe}^{3+}$  in the magma due to the loss of the fluid-mobile  $\text{Fe}^{2+}$ . The near absence of oscillatory zoning might suggest that this pyrochlore crystallised from a turbulent magma (see above), but we think it more likely that the reason for this absence was that pyrochlore and other minerals in the magnetite-biotite rock crystallised during settling under gravity, thereby precluding formation of a boundary layer.

As discussed earlier, some pyrochlore is hosted by the carbonate fraction of the banded carbonatites and late dolomite carbonatites. The pyrochlore occurs mostly in fragments of biotitite and apatitite or as isolated crystals, particularly where the apatite fragments have disaggregated due to apatite dissolution. This and the fact that, compositionally, the pyrochlore hosted by the carbonate fraction of the banded carbonatite and late dolomite carbonatite covers the full range of compositions and types of pyrochlore observed in the other rock units, indicates that most and perhaps all the carbonate-hosted pyrochlore was mechanically introduced from other units.

## **Alteration of pyrochlore**

Several types of pyrochlore alteration were observed, i.e., resorption of the cores, partial or complete replacement by columbite-(Fe), alteration along radial fractures and finally, the formation of patches of clear pyrochlore with or without inclusions of other minerals (e.g., baddeleyite, see above). We attribute the resorption of the pyrochlore cores to disequilibrium among the magma, crystals and exsolved fluid. This fluid was also involved in partial recrystallisation of the cores and the nucleation and growth of baddeleyite. The radial fractures in the Type-2 pyrochlore surrounding cores of Ta-U-rich Type-1 pyrochlore in apatitite are

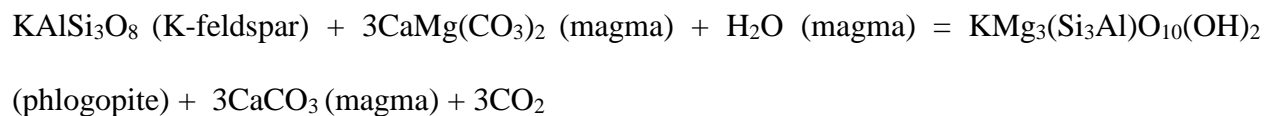
interpreted to have been created by the swelling of the Type-1 pyrochlore during metamictisation. This facilitated the infiltration of a late fluid that post-dated crystallisation of Type-1 and Type-2 pyrochlore (and fluid exsolution) and was responsible for the colourless patchy alteration and the replacement of pyrochlore by columbite-(Fe). A similar proposal was put forward by Duran et al. (2016) to explain the radial fracturing and alteration surrounding euxenite in granitic pegmatites. Further detail on the alteration of pyrochlore to columbite-(Fe) at St Honoré can be found in Tremblay et al. (2017).

### **The origin of the biotitite, apatitite and magnetite-biotite rock**

As mentioned earlier, pyrochlore is extremely soluble (percentage level) in carbonatitic magmas (Jago and Gittins, 1993; Mitchell and Kjarsgaard, 2002; Mitchell and Kjarsgaard, 2004) and, consequently, a carbonatitic magma originating by direct partial melting of the mantle, with a Nb concentration of  $\leq 300$  ppm (Chakhmouradian, 2006; Williams-Jones and Vasyukova, 2022), is significantly undersaturated in pyrochlore. In order to saturate the magma in pyrochlore, much of the magma needs to be consumed. Currently, the only process that has been proposed to achieve this is fractional crystallisation, i.e., crystallisation of calcite or dolomite. Based on the observations presented in this paper, we believe that two other processes, namely, biotitisation (by the magma) and fluid exsolution, were also crucial for the saturation of pyrochlore in the St Honoré carbonatite. Biotitisation was intense at St Honoré and its effect is evident from the presence of massive, fine-grained biotitite, which may extend tens of metres into the host rock (K-rich syenite) from its contact with the carbonatite. Moreover, this massive biotitite contains fine-grained pyrochlore, implying a direct link between the crystallisation of biotite and the saturation of the magma in pyrochlore. As discussed below, we believe that biotitisation was the result of the alteration of the K-feldspar by a dolomite carbonatitic magma and that this reduced the mass of the magma by up to ~50 mol.%, inducing saturation in pyrochlore. The important role played by fluid exsolution in pyrochlore crystallisation is evident from the occurrence of fluid inclusions in apatite that crystallised concurrently with pyrochlore and the composition of the Type-2 pyrochlore (see above). This role of aqueous fluids in pyrochlore crystallisation is consistent with the extremely high solubility of H<sub>2</sub>O in carbonatitic magmas, i.e., ~15 wt.% at 2 kbar and potentially much higher at higher pressure (Keppler, 2003). Thus, fluid exsolution, would have led to a further reduction in the mass of the magma of up to 15 wt.%, ensuring the continued saturation

of pyrochlore. The model that describes the role of each of the processes referred to above is presented in the following paragraphs.

Features that characterise carbonatitic magmas and distinguish them from silicate magmas are their very low viscosity (Genge et al., 1995) and the fact that they are introduced into the host rocks in large numbers of very small batches (Vasyukova and Williams-Jones, 2022). Such features make formation of large carbonatitic magma chambers very unlikely and, instead, promote an interaction of the carbonatitic magmas with their hosts, as suggested for several carbonatites and reproduced in experiments (Anenburg and Mavrogenes, 2018; Wei et al., 2020; Vasyukova and Williams-Jones, 2022; Vasyukova et al., 2023). As mentioned above, the host rocks at St Honoré (K-rich syenites) were metasomatised by carbonatitic magmas (dolomitic) to produce massive fine-grained biotitite. The extent to which this biotitisation occurred varied enormously from one magma batch to the next and depended on the availability of K-rich syenites with which to react. The biotite was produced by the idealised reaction:



and led to the consumption of MgO and H<sub>2</sub>O and the release of CO<sub>2</sub> from the system (Fig. 10). Taken to completion (complete consumption of the MgCO<sub>3</sub> component), this process would have left a residue representing up to 50 mol.% of the initial magma.

With progressive biotitisation, the CaCO<sub>3</sub> activity of the adjacent carbonatitic magma eventually increased to a level high enough to saturate the magma with calcite. The combined effects of biotitisation and fractional crystallisation of calcite, in turn, saturated the magma with pyrochlore and led to the formation of a biotitite with abundant disseminated pyrochlore (Type-1). As crystallisation of calcite in the system CaCO<sub>3</sub>-MgCO<sub>3</sub> can continue until the solidus is reached, this process would have left behind a residual liquid so enriched in silica, phosphate and iron as to constitute a magma that we propose to call phoscoritic (the magma that crystallised apatitite). This, relatively viscous phoscoritic liquid (inferred from the oscillatory zoned apatitite-hosted pyrochlore and the polymerising effect of the silicate and phosphate components of the magma), or crystal mush mingled with subsequent batches of magma to form the banded carbonatites that



constitute much of the niobium resource at St Honoré. The highly evolved nature of the phoscoritic liquid ensured that it was enriched in Nb and a variety of other incompatible elements (Ta, U, Zr, Sr, Ba, Th, Fe, REE and Cl) and that it saturated with a Type-1 pyrochlore characterised by a much higher concentration of these incompatible elements than the Type-1 pyrochlore in biotitite, which crystallised from a less evolved magma (Fig. 10).

As discussed above, we propose that a key event in the evolution of the carbonatitic magma was the exsolution of an aqueous fluid (this occurred because of the increase in the H<sub>2</sub>O activity that accompanied magma consumption). We propose that this took place during pyrochlore crystallisation in apatitite and biotitite and that it is recorded in the change from Type-1 to Type-2 pyrochlore. The exsolution led to the loss of fluid mobile elements, like Fe<sup>2+</sup>, thereby triggering the crystallisation of magnetite because of the increase in Fe<sup>3+</sup> content, and changing the physicochemical environment substantially. This resulted in the crystallisation of near stoichiometric Type-2 pyrochlore as an overgrowth on Type-1 pyrochlore (Fig. 10).

In addition to exsolving from the magma as a result of crystallisation, an aqueous phase likely exsolved at other stages in the development of the complex as a result of periodic changes in pressure. Thus, in some locations, exsolution of the aqueous fluid could have occurred during or immediately after biotitisation, but before the crystallisation of calcite and the development of a phoscoritic liquid. We propose that, if fluid exsolution occurred before the crystallisation of Type-1 pyrochlore, the magma would have saturated in Type-2 pyrochlore. This explains the absence of Type-1 pyrochlore in the magnetite-biotite rock. It also explains the presence of abundant magnetite in this rock unit, the crystallisation of which was promoted by the high activity of Fe<sup>3+</sup> due to the loss of Fe<sup>2+</sup> to the fluid; the biotite crystallised because of the elevated activity of K, Al and Si adjacent to the biotitite/syenite. Based on the absence of oscillatory zoning in the pyrochlore, crystallisation of magnetite, pyrochlore and biotite is interpreted to have occurred while these minerals settled under gravity (this prevented the development of a boundary layer) to form a magnetite-biotite rock in which the pyrochlore is exclusively the Type-2 variety (Fig. 10).

Although pyrochlore also is present in the carbonate fraction of the banded carbonatite and the late dolomite carbonatite, its concentration in these units is low and several lines of evidence suggest that pyrochlore was mechanically introduced. The evolution of the late carbonate magmas did not

involve metasomatic interaction with the syenite because of previous biotitisation of this unit by earlier batches of carbonatitic magma. In the absence of further concentration of Nb, the late batches of carbonatitic magma most likely evolved by cooling to the liquidus and crystallising as dolomite carbonatite with rare disseminated pyrochlore (Fig. 10).

## Concluding remarks

Experimental studies have shown that the solubility of pyrochlore in carbonatitic magmas is extremely high, i.e., at percentage levels (Jago and Gittins, 1993; Mitchell and Kjarsgaard, 2002; Mitchell and Kjarsgaard, 2004). Given that carbonatitic magmas likely contain only a few hundred ppm of Nb on intrusion, it therefore follows that, initially, the magmas are highly undersaturated in pyrochlore and that pyrochlore cannot be the first mineral on the liquidus (Williams-Jones and Vasyukova, 2022). This conclusion, however, is inconsistent with the textural evidence, namely that pyrochlore typically occurs as euhedra and as inclusions in other (early crystallising) minerals. Based on the data for the St Honoré carbonatite complex, we have developed a model that resolves this issue. We believe that there are three processes, which concentrate niobium in carbonatitic magmas, and cause them to saturate in pyrochlore. These processes are biotitisation, crystallisation of calcite and exsolution of an aqueous fluid. Biotitisation and crystallisation of calcite consume MgO, CaO, H<sub>2</sub>O and CO<sub>2</sub> and lead to the saturation of Ta-U-rich Type-1 pyrochlore. Fluid exsolution removes H<sub>2</sub>O, Cl and fluid-mobile elements (e.g., U, Fe<sup>2+</sup>, Sr and REE) and sharply increases the F/OH ratio, causing the crystallisation of Ta-U-free, F-rich Type-2 pyrochlore. The extent of biotitisation determines whether there is crystallisation of calcite and the formation of a residual phoscoritic magma that saturates in a Type-1 pyrochlore, unusually enriched in Ta and U. Each of the magma batches at St Honoré had a slightly different evolutionary path because of variations in the proportions of fresh syenite available for biotitisation and the timing of fluid exsolution. As a result, there is a remarkable heterogeneity in the mode of occurrence and composition of the pyrochlore. Post-crystallisation mechanical mobilisation by late carbonatitic magma batches and at least two fluid events added further complexity to the resulting textures.

Extreme textural and compositional heterogeneity, and the occurrence of two types of pyrochlore, an early Ta-U variety and a later near end-member fluorcalciopyrochlore, are not restricted to St Honoré. Indeed, most Nb-enriched carbonatites contain these two types of pyrochlore and display a similar complexity of pyrochlore compositions and textures. Equally common is the occurrence

of biotitites and the concentration of the pyrochlore in apatite-rich layers and lenses in banded carbonatites. We, therefore, conclude that the hypotheses presented in this paper are applicable to most carbonatites in which pyrochlore is an important ore mineral, and encourage other researchers investigating pyrochlore-enriched carbonatites to further test and refine the model developed here for carbonatite-hosted niobium mineralisation.

## Acknowledgements

The research presented in this paper was funded by a grant from Niobec<sup>Nb</sup> and a Discovery grant from the National Scientific and Engineering Research Council of Canada (NSERC). The support provided by the geological staff of Niobec<sup>Nb</sup> (Guillaume Matton, Alexis Gauthier-Ross, Christian Beaulieu and Marc Lavoie) and the opportunity to discuss with them the ideas presented in this paper are gratefully acknowledged. The constructive comments of one of two anonymous referees and Editor-in-Chief Karen Johannesson are gratefully acknowledged and helped improve the manuscript significantly.

## Figure captions

Figure 1. A schematic geological map of the St Honoré carbonatite modified from an unpublished map supplied by Niobec<sup>Nb</sup>.

Figure 2. Photographs of drill core from the St Honoré carbonatite. (a) – altered syenite displaying weak biotitisation, (b) – biotitite (intense biotitisation) cut by a pyrite-bearing dolomite vein, (c) – the magnetite-rich variety of the magnetite-biotite rock, (d) – the biotite-rich variety of the magnetite-biotite rock, (e) – banded calcite carbonatite containing a large apatite lens and (f) – a dykelet of grey dolomite carbonatite cutting light-coloured banded dolomite carbonatite containing small fragments of biotitised syenite.

Figure 3. A Ca-Na-A-site vacancy diagram showing the distribution of pyrochlore compositions in apfu of the different rock units. Also shown are the fields of calciopyrochlore (Ca-Pyr), natropyrochlore (Na-Pyr) and kenopyrochlore (Ke-Pyr).

Figure 4. Modes of pyrochlore occurrence in the biotitite. (a-d) – transmitted light photomicrographs: (a) – biotite-hosted pyrochlore crystals (partly chloritised), isolated

or aggregates. Note that the pyrochlore is surrounded by haloes of radiation damage. (b) – biotite- and magnetite-associated pyrochlore in a sample displaying intense biotitisation, (c) – the area of the white rectangle in (b) showing tiny biotite-associated pyrochlore grains (blue arrows) with haloes of radiation damage and larger magnetite-associated pyrochlore containing inclusions of biotite (red outlines). (d) – replacement of perthite by fine-grained biotite and a concentration of pyrochlore at the contact between this biotite and coarse-grained biotite, which passes outwards into dolomite carbonatite. (e-f) – BSE images: (e) – the area of the white rectangle in (d) showing a layer of pyrochlore aggregates at the contact between fine-grained biotite and coarse-grained biotite, (f) – the area of the black rectangle in (e) showing bright pyrochlore cores surrounded by darker rims (see the main text for further detail). Bt – biotite, Chl – chlorite, Dol – dolomite, Mgt – magnetite, Pyr – pyrochlore.

Figure 5. Triangular diagrams showing the distribution of pyrochlore compositions (apfu) for the crystals from different rock units. (a) – Ca+Na vs. Ta and U, (b) – Ca+Na vs. A-site vacancy and F and (c) – Nb vs. Ti+Zr+Si and Ta.

Figure 6. Images of pyrochlore in magnetite-biotite rock: (a) – a transmitted light photomicrograph showing textural relationships among biotite, magnetite, pyrochlore (patchy) and dolomite. (b) – a transmitted light photomicrograph showing a euhedral crystal of pyrochlore with colourless alteration concentrated in patches near its rim, (c) – a transmitted light photomicrograph of an example of an oscillatory zoned (rare) Type-2 pyrochlore crystal that has been extensively altered to colourless fluorcalciopyrochlore and locally columbite-(Fe). (d) – a BSE image of a partially altered Type-2 pyrochlore containing patches of columbite-(Fe) and baddeleyite. Bd – baddeleyite, Bt – biotite, Col – columbite-(Fe), Dol – dolomite, Mgt – magnetite and Pyr – pyrochlore.

Figure 7. Modes of occurrence of pyrochlore in apatite shown in transmitted light. (a) – dolomite carbonatite-hosted apatite containing subhedral to euhedral pyrochlore crystals of variable size with apatite inclusions in their outer parts. The large crystal contains a distinctive (yellow to red-brown) core, but the other crystals do not contain distinguishable cores. (b) – calcite carbonatite-hosted apatite containing small

pyrochlore euhedra. (c) – a large pyrochlore crystal with a partially resorbed core in apatite hosted by calcite carbonatite. The rim of the pyrochlore is oscillatory zoned and contains numerous radial fractures. (d) – a large complexly zoned pyrochlore crystal comprising a core with three zones overgrown by later pyrochlore in apatite hosted by dolomite carbonatite (see main text for further description). A BSE image of the same crystal is shown in the inset. (e) – part of a large pyrochlore crystal containing inclusions of fluid inclusion-bearing apatite in apatite hosted by dolomite carbonatite. The inset of the area outlined in black shows a fluid inclusion containing a vapour bubble and two anisotropic solids. Ap – apatite, Bt – biotite, Dol – dolomite, Mgt – magnetite, Pyr – pyrochlore.

Figure 8. A triangular diagram with Ca+Na – U – Ta coordinates showing the composition of the zones in apatite-hosted pyrochlore crystals of the type illustrated in Figure 7d. The dashed lines illustrate the compositional trends of the two varieties of pyrochlore identified in BSE images (see main text for further detail).

Figure 9. Modes of occurrence of pyrochlore hosted by the carbonate fraction of the banded carbonatite and the late dolomite carbonatite. (a) – a transmitted light photomicrograph showing a pyrochlore hosted by a fragment of apatite within late dolomite carbonatite. (b) – the same image in crossed polarised light. (c) – a transmitted light photomicrograph of a partially disaggregated fragment of apatite containing pyrochlore in a matrix of late dolomite carbonatite. (d) – the same image in crossed polarised light. (e) – a transmitted light photomicrograph showing two apatite crystals containing small inclusions of pyrochlore in dolomite carbonatite and two isolated pyrochlore crystals in dolomite adjacent to the apatite. (f) – a transmitted light photomicrograph showing an inclusion of pyrochlore and an inclusion of columbite-(Fe) after pyrochlore in dolomite. Two other columbite-(Fe) crystals are adjacent to the dolomite crystal. The host is a late dolomite carbonatite. Ap – apatite, Bt – biotite, Col – columbite-(Fe), Dol – dolomite, Pyr – pyrochlore.

Figure 10. A schematic diagram illustrating the evolution of the St Honoré carbonatitic magma and the processes controlling the formation of different units (see the main text for further detail).

## References

- Anenburg, M., and Mavrogenes, J. A., 2018, Carbonatitic versus hydrothermal origin for fluorapatite REE-Th deposits: Experimental study of REE transport and crustal “antiskarn” metasomatism: *American Journal of Science*, v. 318, p. 335-366.
- Atencio, D., Andrade, M. B., Christy, A. G., Gieré, R., and Kartashov, P. M., 2010, The pyrochlore supergroup of minerals: nomenclature: *The Canadian Mineralogist*, v. 48, p. 673-698.
- Chakhmouradian, A., Williams, C., Wall, F., and Zaitsev, A., 2004, Mineralogy of high-field-strength elements (Ti, Nb, Zr, Ta, Hf) in phoscoritic and carbonatitic rocks of the Kola Peninsula, Russia: Phoscorites and carbonatites from mantle to mine: the key example of the Kola Alkaline Province, v. 10, p. 293-340.
- Chakhmouradian, A. R., 2006, High-field-strength elements in carbonatitic rocks: geochemistry, crystal chemistry and significance for constraining the sources of carbonatites: *Chemical Geology*, v. 235, p. 138-160.
- Chakhmouradian, A. R., Reguir, E. P., Kressall, R. D., Crozier, J., Pisiak, L. K., Sidhu, R., and Yang, P., 2015, Carbonatite-hosted niobium deposit at Aley, northern British Columbia (Canada): Mineralogy, geochemistry and petrogenesis: *Ore Geology Reviews*, v. 64, p. 642-666.
- Chakhmouradian, A. R., and Williams, C. T., 2004, Mineralogy of high-field-strength elements (Ti, Nb, Zr, Ta, Hf) in phoscoritic and carbonatitic rocks of the Kola Peninsula, Russia, *in* Wall, F., and Zaitsev, A. N., eds., Phoscorites and carbonatites from mantle to mine: the key example of the Kola alkaline province, Mineralogical Society of Great Britain and Ireland, p. 293-340.
- da Costa, I. R., Roseiro, J., Figueiras, J., Rodrigues, P., and Mateus, A., 2021, Pyrochlore from the Bailundo Carbonatite Complex (Angola): Compositional variation and implications to mineral exploration: *Journal of African Earth Sciences*, v. 177, p. 104154.
- Dey, M., Bhattacharjee, S., Chakrabarty, A., Mitchell, R. H., Pal, S., Pal, S., and Sen, A. K., 2021, Compositional variation and genesis of pyrochlore, belkovite and baotite from the Sevattur carbonatite complex, India: *Mineralogical Magazine*, v. 85, p. 588-606.
- Duran, C. J., Seydoux-Guillaume, A.-M., Bingen, B., Gouy, S., De Parseval, P., Ingrin, J., and Guillaume, D., 2016, Fluid-mediated alteration of (Y, REE, U, Th)–(Nb, Ta, Ti) oxide minerals in granitic pegmatite from the Evje-Iveland district, southern Norway: *Mineralogy and Petrology*, v. 110, p. 581-599.

- 645 Genge, M. J., Price, G. D., and Jones, A. P., 1995, Molecular dynamics simulations of  $\text{CaCO}_3$   
646 melts to mantle pressures and temperatures: implications for carbonatite magmas: *Earth*  
647 and Planetary Science Letters, v. 131, p. 225-238.
- 648 Guarino, V., Wu, F.-Y., Melluso, L., de Barros Gomes, C., Tassinari, C. C. G., Ruberti, E., and  
649 Brilli, M., 2017, U–Pb ages, geochemistry, C–O–Nd–Sr–Hf isotopes and petrogenesis of  
650 the Catalão II carbonatitic complex (Alto Paranaíba Igneous Province, Brazil):  
651 implications for regional-scale heterogeneities in the Brazilian carbonatite associations:  
652 *International Journal of Earth Sciences*, v. 106, p. 1963-1989.
- 653 Hogarth, D., Williams, C., and Jones, P., 2000, Primary zoning in pyrochlore group minerals from  
654 carbonatites: *Mineralogical Magazine*, v. 64, p. 683-697.
- 655 Jago, B., and Gittins, J., 1993, Pyrochlore crystallization in carbonatites: the role of fluorine: *South*  
656 *African Journal of Geology*, v. 96, p. 149-160.
- 657 Keppler, H., 2003, Water solubility in carbonatite melts: *American Mineralogist*, v. 88, p. 1822-  
658 1824.
- 659 Kjarsgaard, B. A., and Mitchell, R. H., 2008, Solubility of Ta in the system  $\text{CaCO}_3\text{--Ca}(\text{OH})_2\text{--}$   
660  $\text{NaTaO}_3\text{--NaNbO}_3\pm\text{F}$  at 0.1 GPa: implications for the crystallization of pyrochlore-group  
661 minerals in carbonatites: *The Canadian Mineralogist*, v. 46, p. 981-990.
- 662 Lee, M. J., Lee, J. I., Garcia, D., Moutte, J., Williams, C. T., Wall, F., and Kim, Y., 2006,  
663 Pyrochlore chemistry from the Sokli phoscorite-carbonatite complex, Finland:  
664 implications for the genesis of phoscorite and carbonatite association: *Geochemical*  
665 *Journal*, v. 40, p. 1-13.
- 666 McCausland, P. J., Pisarevsky, S., Jourdan, F., and Higgins, M., 2009, Laurentia at 571 Ma:  
667 Preliminary paleomagnetism and Ar–Ar age of the Ediacaran St Honore alkaliintrusion,  
668 Quebec: AGU spring meeting, Toronto, 2009.
- 669 Mitchell, R. H., 2015, Primary and secondary niobium mineral deposits associated with  
670 carbonatites: *Ore Geology Reviews*, v. 64, p. 626-641.
- 671 Mitchell, R. H., and Kjarsgaard, B. A., 2002, Solubility of niobium in the system  $\text{CaCO}_3\text{--}$   
672  $\text{Ca}(\text{OH})_2\text{--NaNbO}_3$  at 0.1 GPa pressure: *Contributions to Mineralogy and Petrology*, v. 144,  
673 p. 93-97.
- 674 Mitchell, R. H., and Kjarsgaard, B. A., 2004, Solubility of niobium in the system  $\text{CaCO}_3\text{--CaF}_2\text{--}$   
675  $\text{NaNbO}_3$  at 0.1 GPa pressure: implications for the crystallization of pyrochlore from  
676 carbonatite magma: *Contributions to Mineralogy and Petrology*, v. 148, p. 281-287.
- 677 Mitchell, R. H., Wahl, R., and Cohen, A., 2020, Mineralogy and genesis of pyrochlore apatite  
678 from The Good Hope Carbonatite, Ontario: A potential niobium deposit: *Mineralogical*  
679 *Magazine*, v. 84, p. 81-91.

- 680 Thivierge, S., Roy, D.-W., Chown, E., and Gauthier, A., 1983, Évolution du complexe alcalin de  
681 St.-Honoré (Québec) après sa mise en place: *Mineralium Deposita*, v. 18, p. 267-283.
- 682 Tremblay, J., Bédard, L. P., and Matton, G., 2017, Columbitization of fluorcalciopyrochlore by  
683 hydrothermalism at the Saint-Honoré alkaline complex, Québec (Canada): New insights  
684 on halite in carbonatites: *Ore Geology Reviews*, v. 91, p. 695-707.
- 685 Vallières, D., Pelletier, P., Gaultier, P., Ferlatte, G., Tremblay, J.-F., and Sirois, R., 2013, NI 43-  
686 101 Technical Report, Update on Niobec Expansion, December 2013.
- 687 Vasyukova, O., Kostyuk, A., and Williams-Jones, A., 2023, Kovdor to Oldoinyo Lengai—The  
688 missing link in carbonatitic magma evolution: *Geology*, v. 51, p. 59-63.
- 689 Vasyukova, O. V., and Williams-Jones, A. E., 2022, Carbonatite metasomatism, the key to  
690 unlocking the carbonatite-phoscorite-ultramafic rock paradox: *Chemical Geology*, v. 602,  
691 p. 120888.
- 692 Walter, B., Parsapoor, A., Braunger, S., Marks, M., Wenzel, T., Martin, M., and Markl, G., 2018,  
693 Pyrochlore as a monitor for magmatic and hydrothermal processes in carbonatites from the  
694 Kaiserstuhl volcanic complex (SW Germany): *Chemical Geology*, v. 498, p. 1-16.
- 695 Wei, C.-W., Xu, C., Chakhmouradian, A. R., Brenna, M., Kynicky, J., and Song, W.-L., 2020,  
696 Carbon–strontium isotope decoupling in carbonatites from Caotan (Qinling, China):  
697 implications for the origin of calcite carbonatite in orogenic settings: *Journal of Petrology*,  
698 v. 61, p. egaa024.
- 699 Williams-Jones, A. E., and Vasyukova, O. V., 2022, Niobium, Critical Metal and Progeny of the  
700 Mantle: *Economic Geology*, v. doi:10.5382/econgeo.4994.
- 701 Zaitsev, A. N., Spratt, J., Shtukenberg, A. G., Zolotarev, A. A., Britvin, S. N., Petrov, S. V.,  
702 Kuptsova, A. V., and Antonov, A. V., 2021, Oscillatory-and sector-zoned pyrochlore from  
703 carbonatites of the Kerimasi volcano, Gregory rift, Tanzania: *Mineralogical Magazine*, v.  
704 85, p. 532-553.
- 705 Zurevinski, S. E., and Mitchell, R. H., 2004, Extreme compositional variation of pyrochlore-group  
706 minerals at the Oka carbonatite complex, Quebec: evidence of magma mixing?: *The*  
707 *Canadian Mineralogist*, v. 42, p. 1159-1168.

708

709



Figure 1

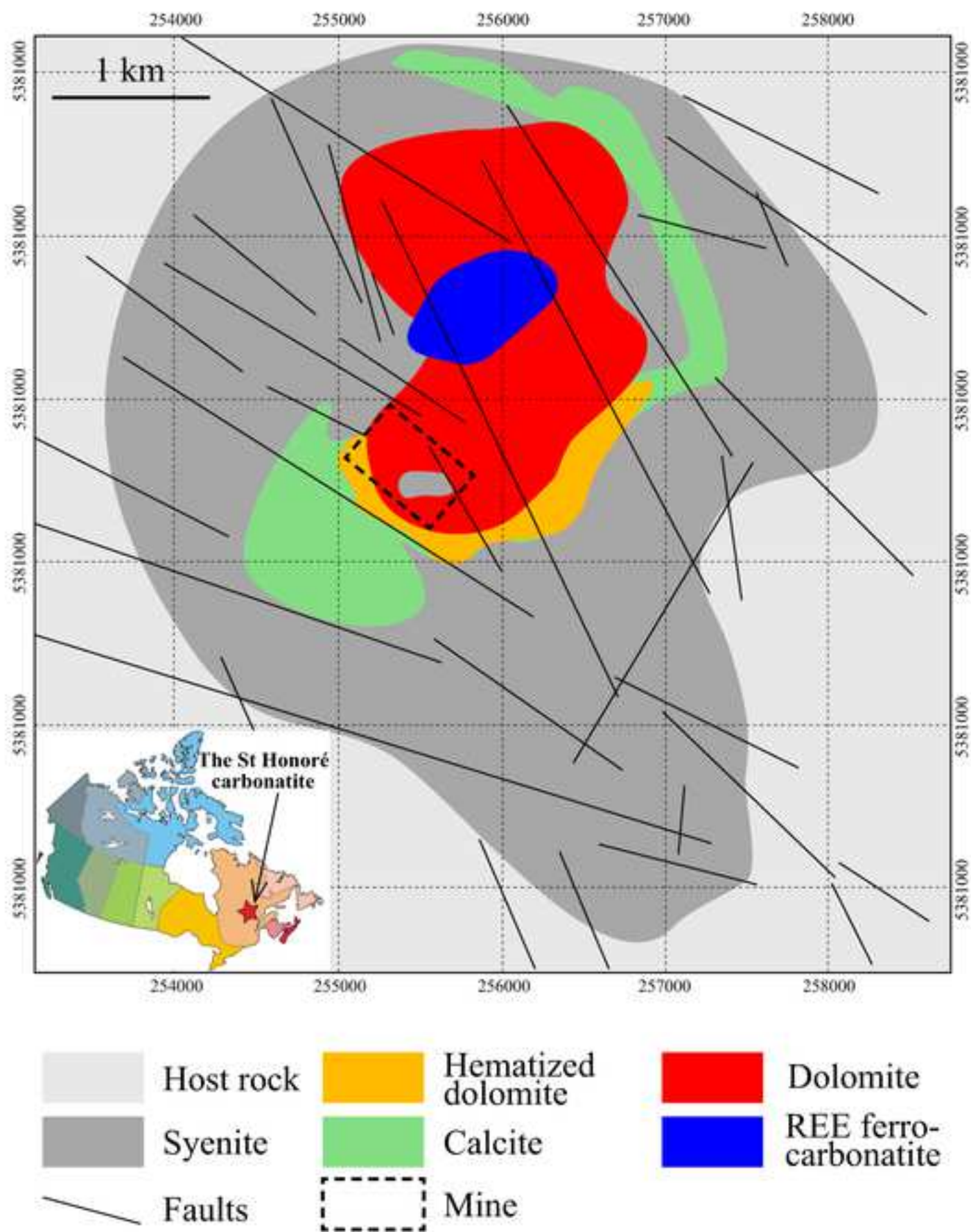




Figure 2

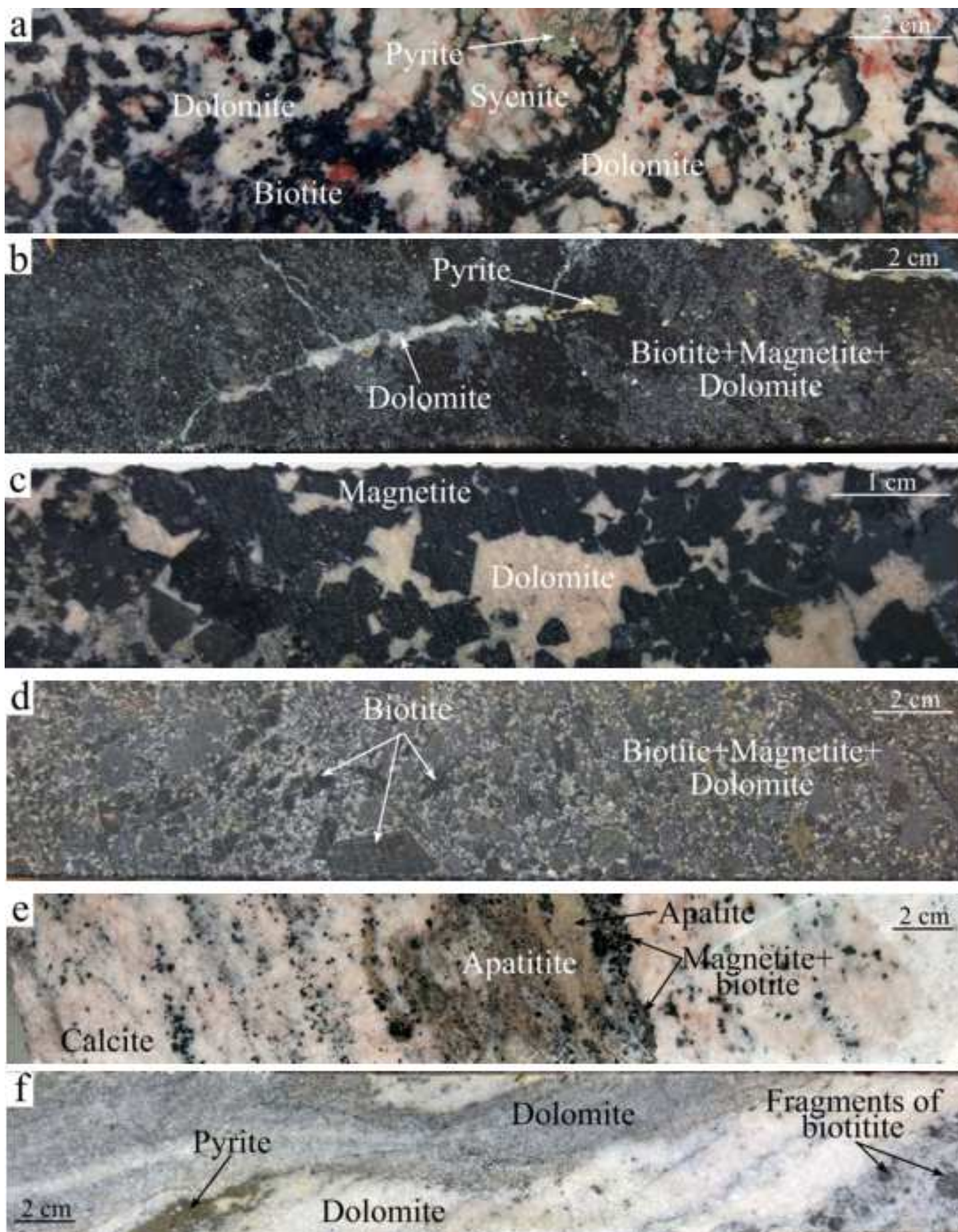


Figure 3

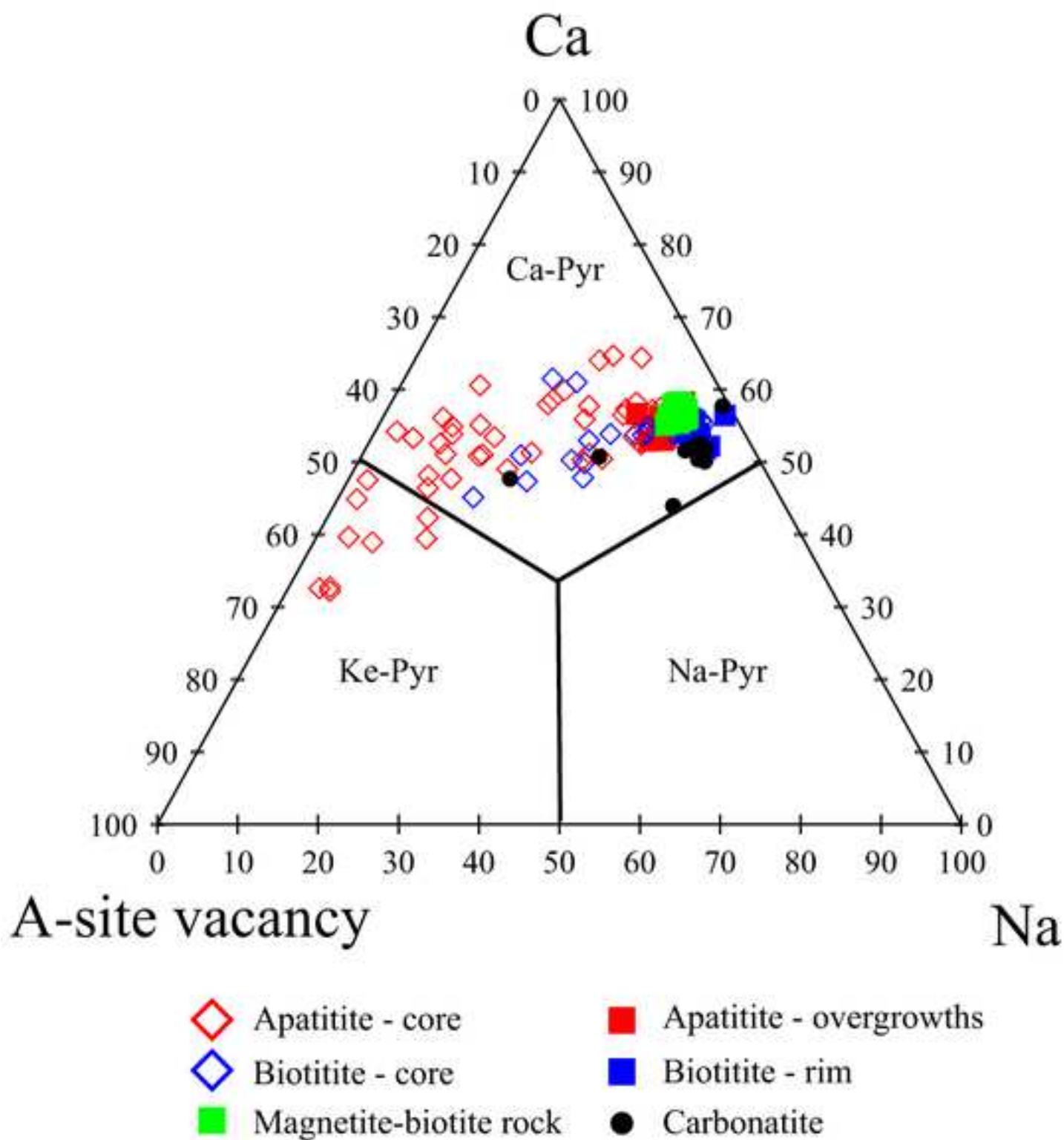




Figure 4

[Click here to access/download;Figure;Pyrochlore\\_R1\\_4 copy.TIF](#)

Vasyukova, O., and Williams-Jones, A., 2023, A new model for the origin of pyrochlore:  
Evidence from the St Honoré Carbonatite, Canada: *Chemical Geology*, p. 121549.

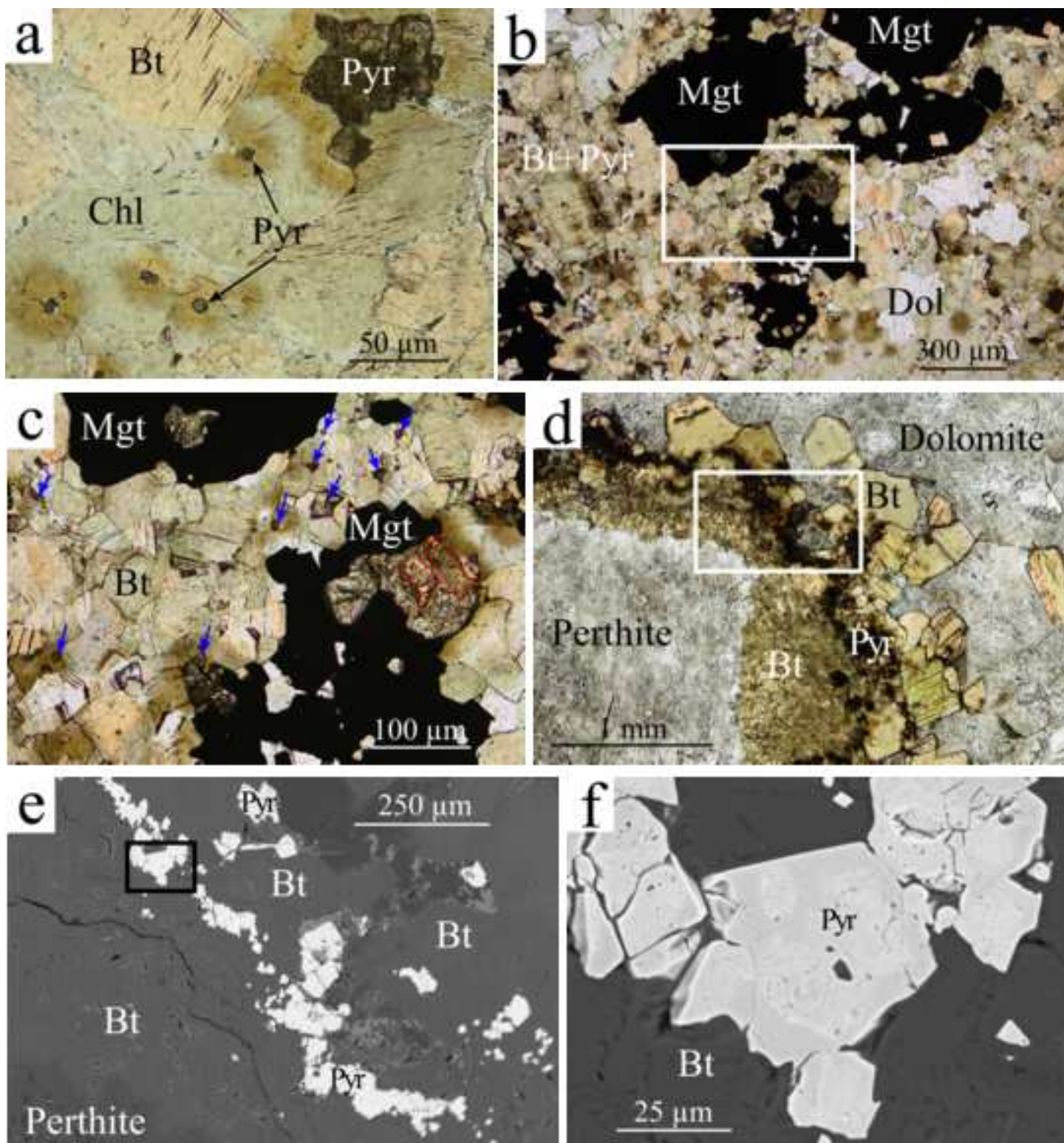


Figure 5

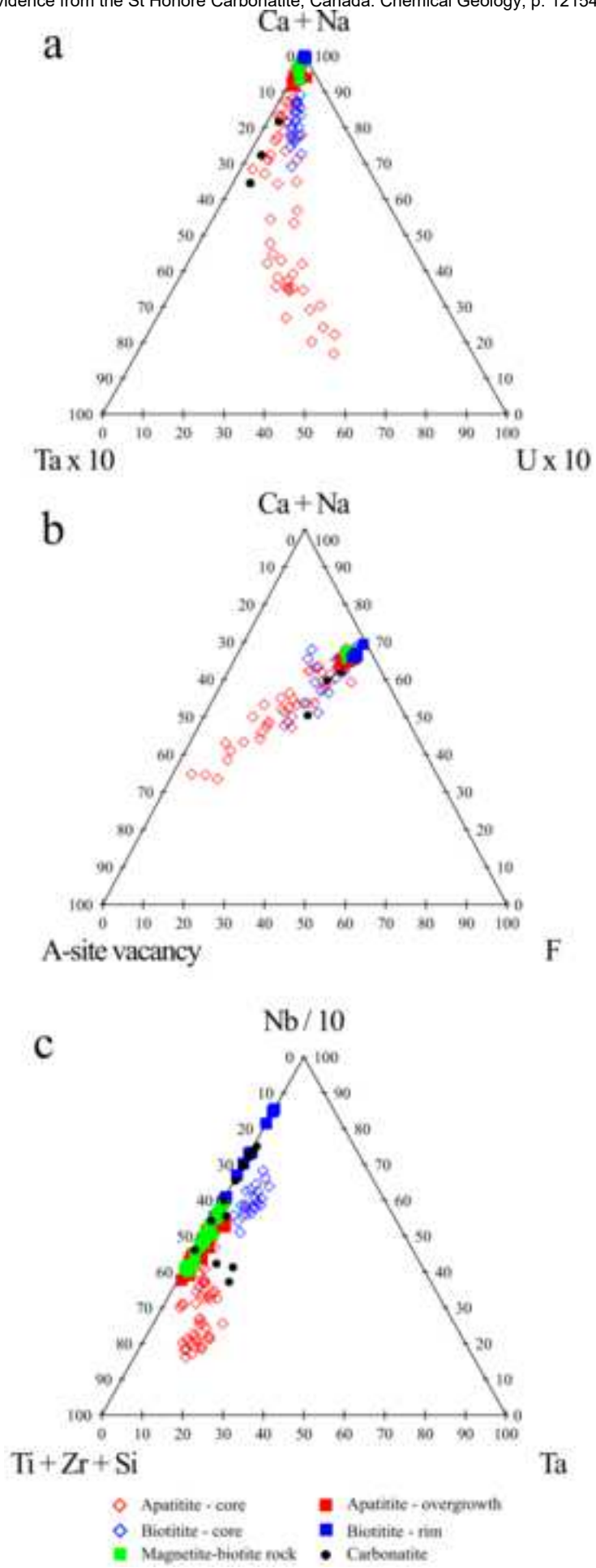




Figure 6

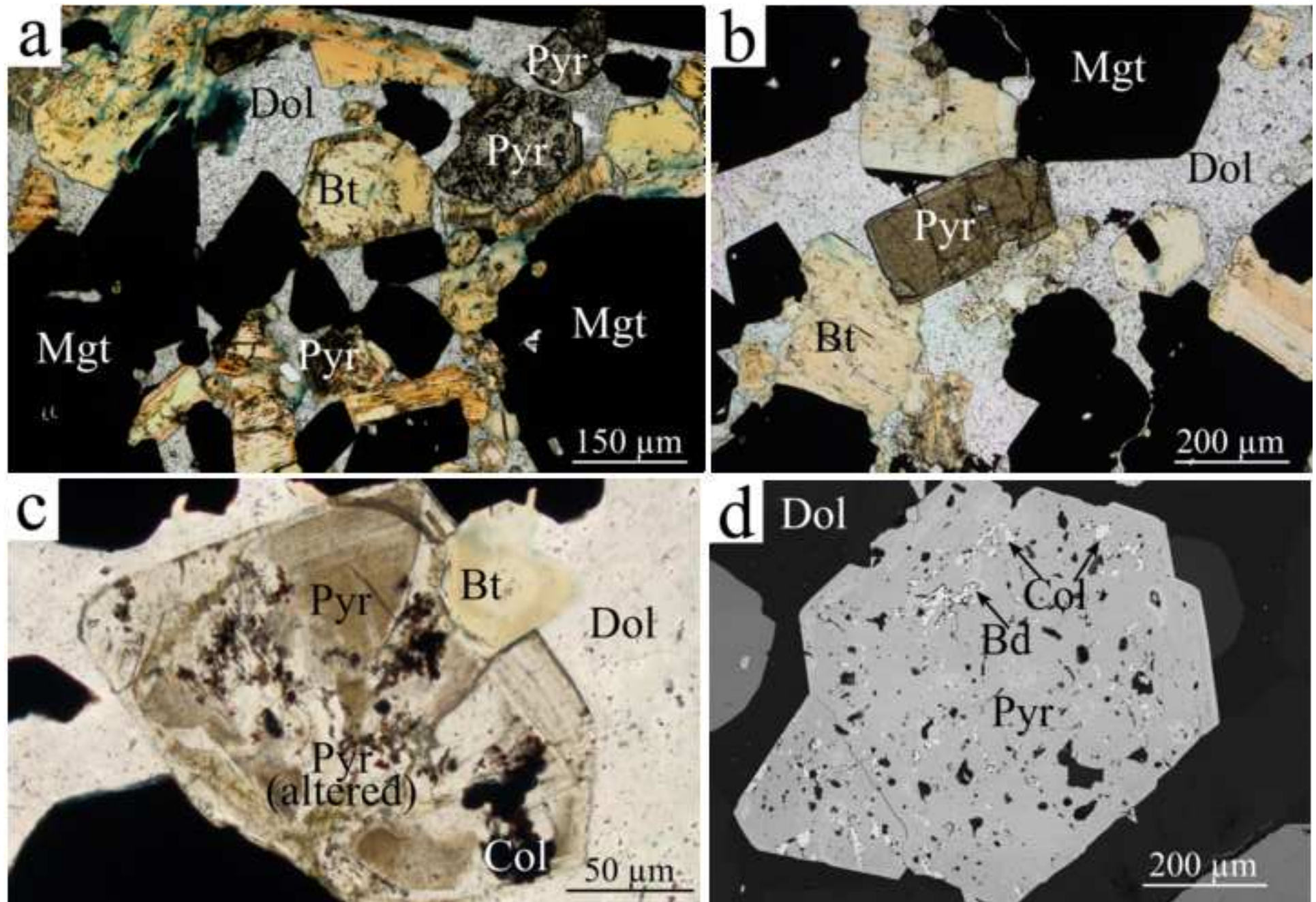




Figure 7

[Click here to access/download;Figure;Pyrochlore\\_R1\\_7 copy.TIF](#)

Vasyukova, O., and Williams-Jones, A., 2023, A new model for the origin of pyrochlore:  
Evidence from the St Honoré Carbonatite, Canada: *Chemical Geology*, p. 121549.

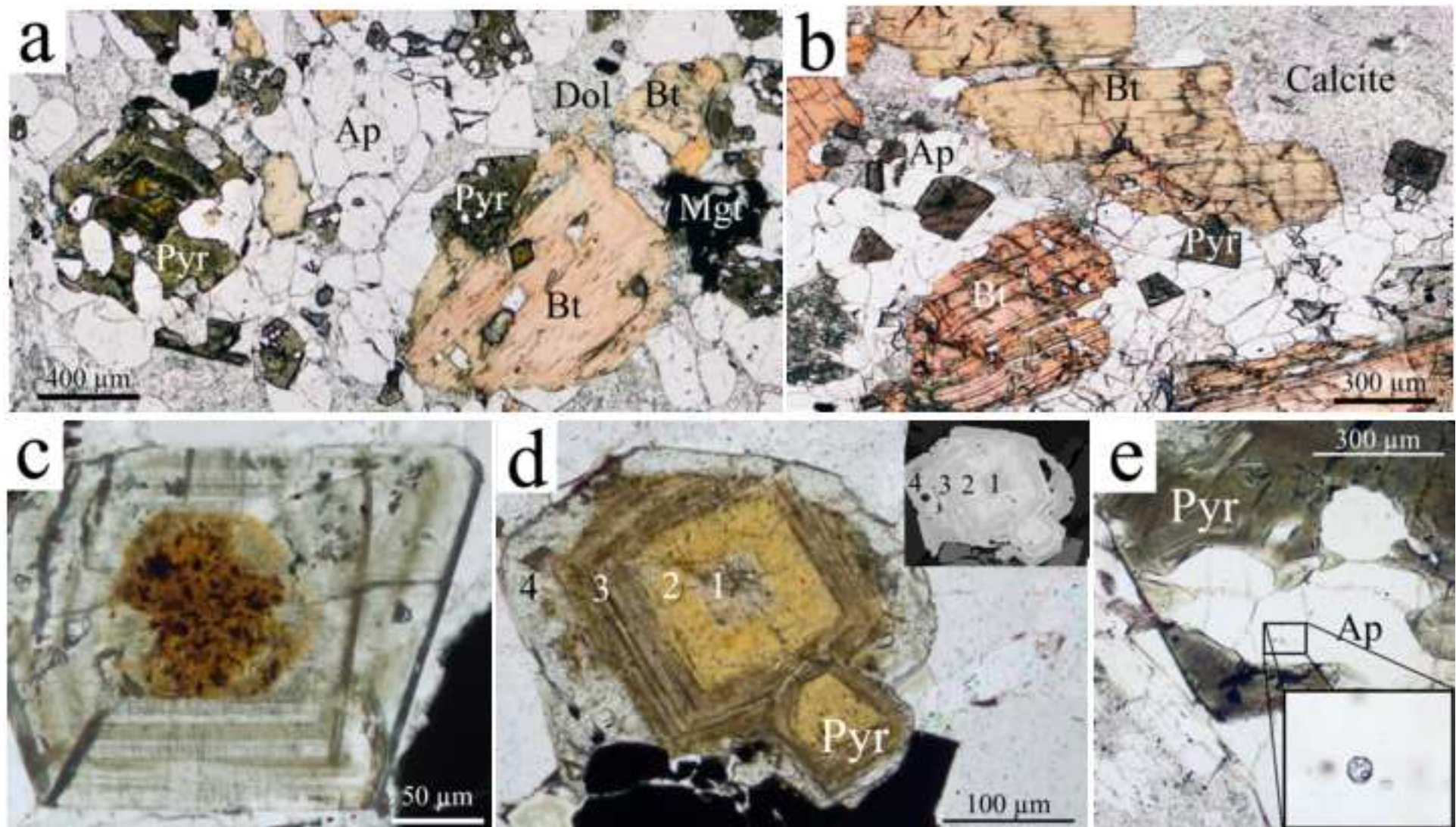


Figure 8

Vasyukova, O., and Williams-Jones, A., 2023, A new model for the origin of pyrochlore:  
Evidence from the St Honoré Carbonatite, Canada: Chemical Geology, p. 121549.

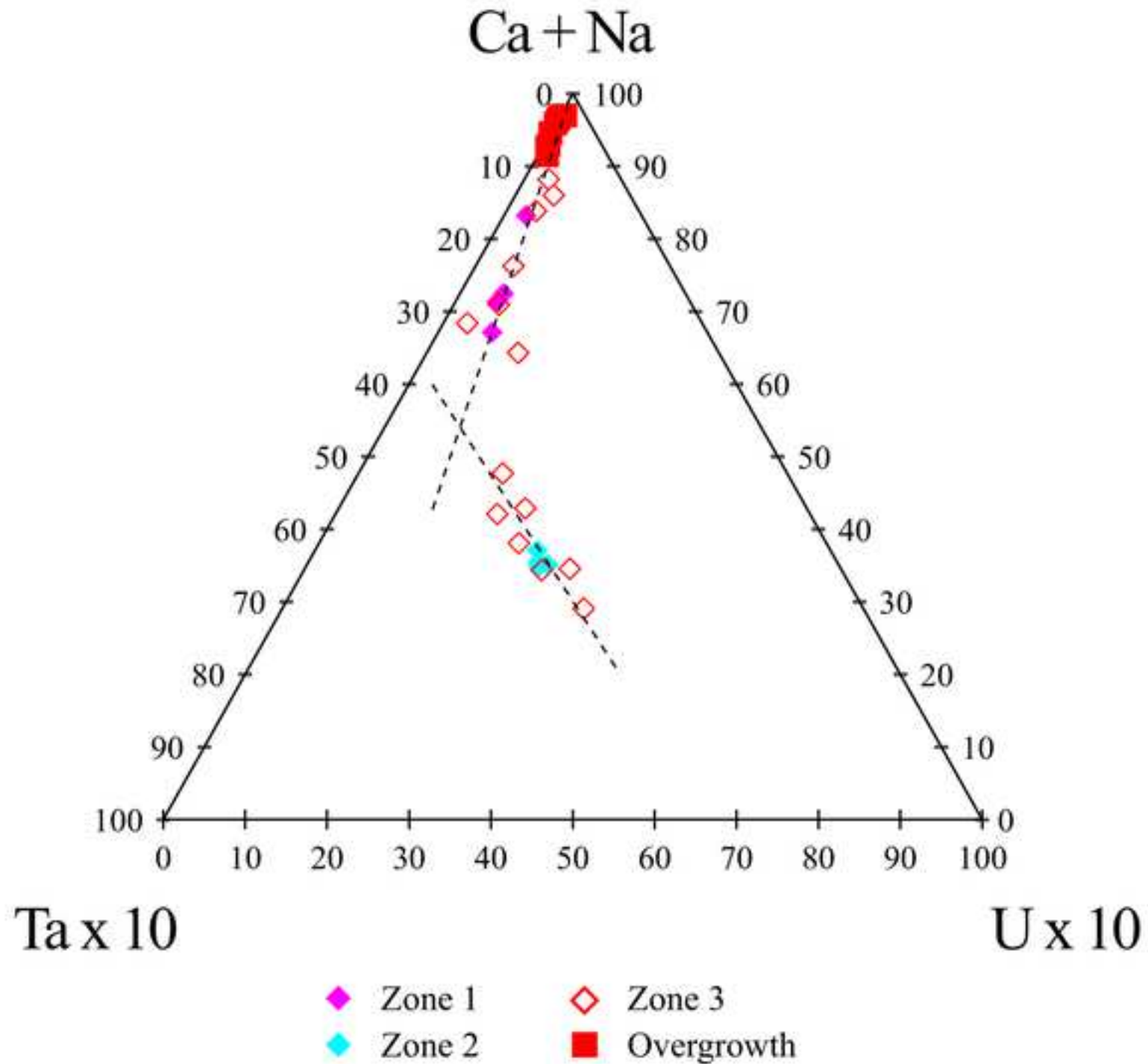
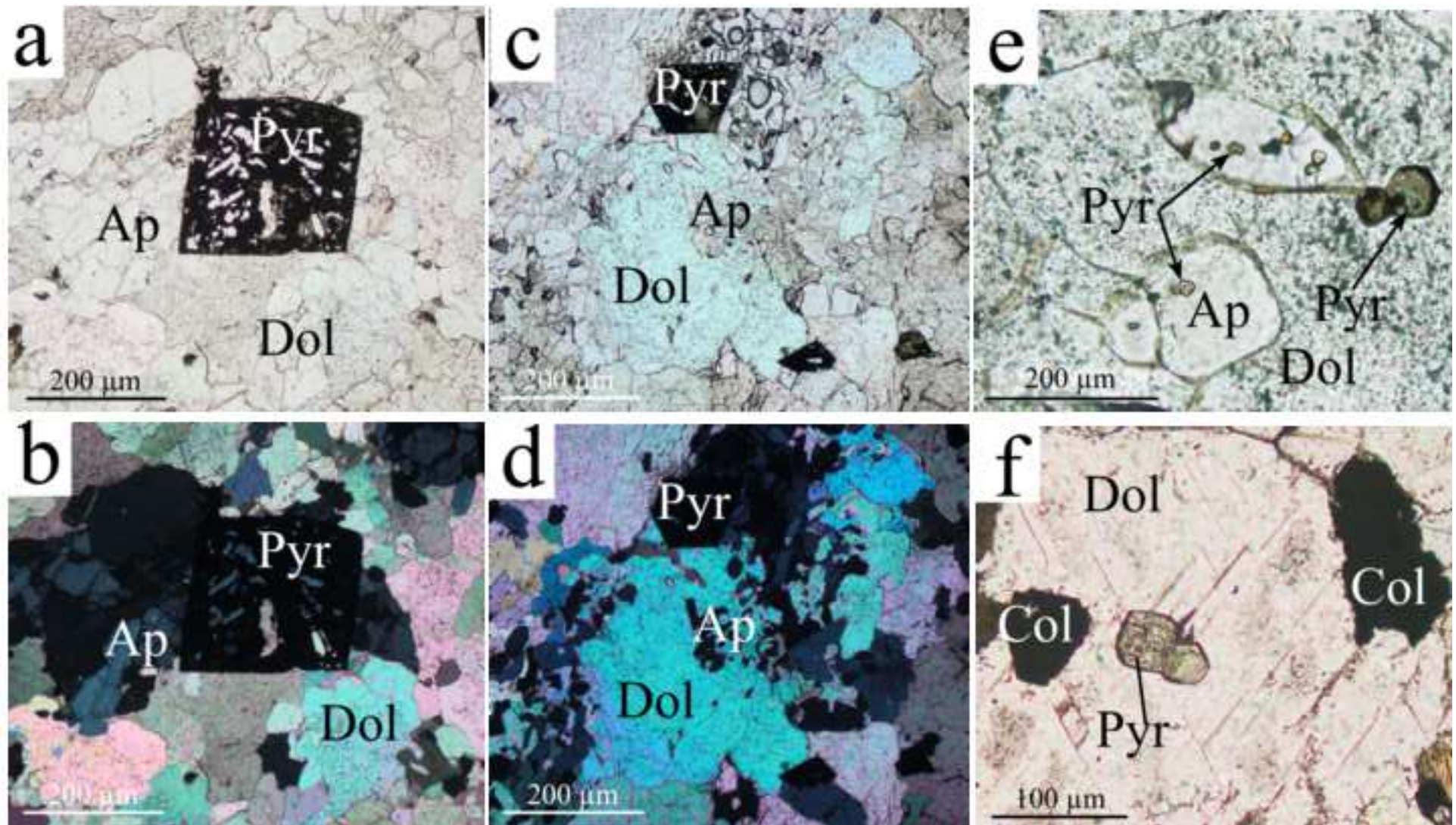




Figure 9



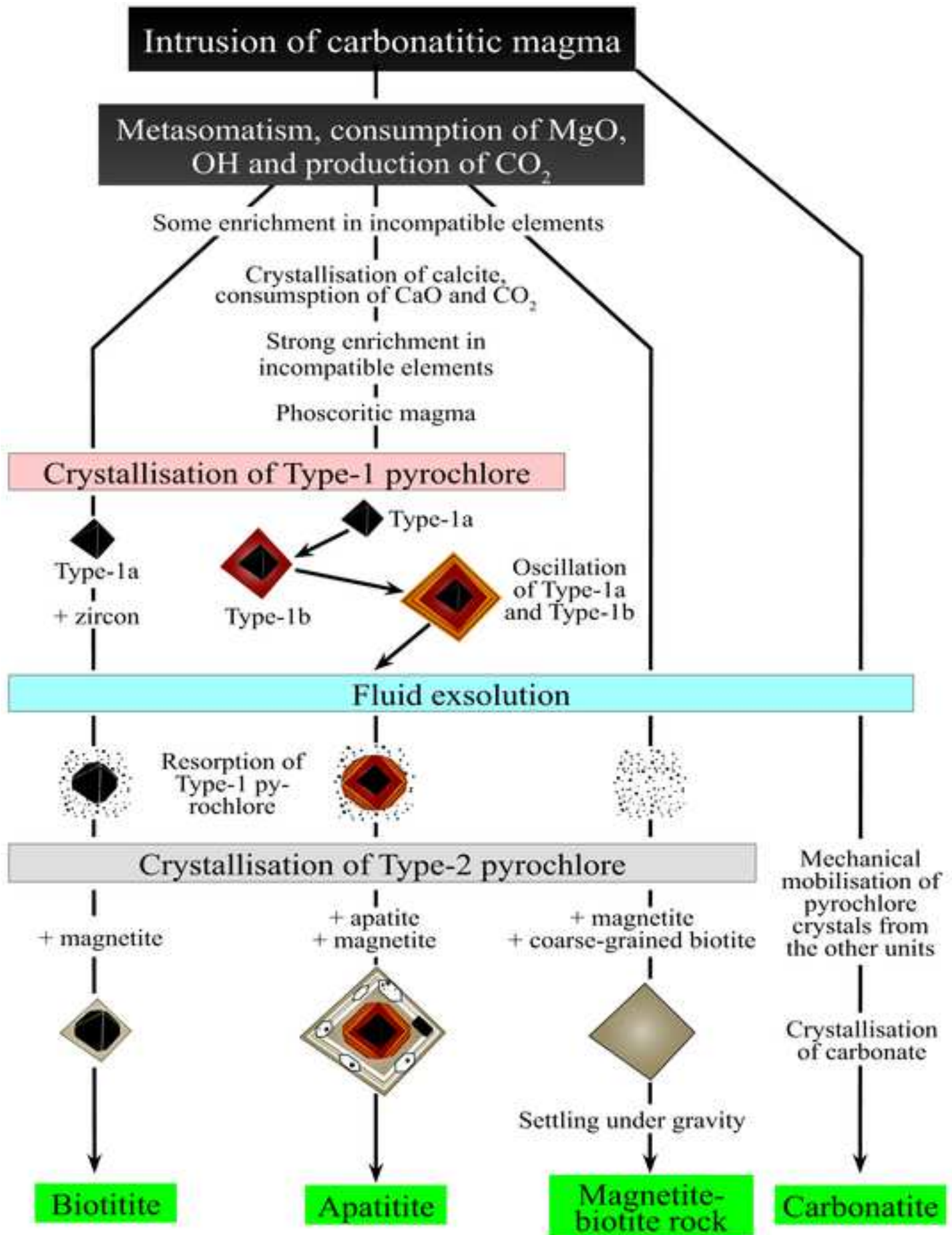




Table 1. Average compositions (wt.% and apfu) of pyrochlore in biotitite, magnetite-biotite rock, apatitite and ca

	Biotitite				Magnetite-biotite rock				Apatitite		
	Cores		Rims				Zone 1		Zone 2		Zone 3
# analyses	22	sd	14	sd	30	sd	4	sd	15	sd	26
Nb <sub>2</sub> O <sub>5</sub>	67.6	0.8	69.3	1.1	66.2	1.3	61.4	0.7	48.9	3.0	57.3
Ta <sub>2</sub> O <sub>5</sub>	1.4	0.3			0.2	0.1	2.7	0.6	5.2	0.9	2.8
TiO <sub>2</sub>	2.0	0.4	1.8	0.8	3.4	0.4	3.9	0.2	5.0	0.9	4.1
ZrO <sub>2</sub>			0.1	0.1	0.7	0.6	2.5	0.2	2.8	1.7	2.1
SiO <sub>2</sub>	0.2	0.2	0.1	0.0	0.2	0.3	0.2	0.1	2.0	0.9	1.1
CaO	15.2	1.0	16.1	0.7	17.0	0.5	15.1	0.3	10.6	2.1	14.1
Na <sub>2</sub> O	4.9	1.2	6.5	0.2	6.0	0.1	4.6	0.8	0.9	0.5	3.2
FeO	0.8	0.6	0.3	0.5	0.2	0.2	0.4	0.1	3.1	1.0	1.5
SrO	1.3	0.5	1.0	0.1	0.5	0.1	0.6	0.1	2.2	0.8	1.4
UO <sub>2</sub>	1.1	0.3					0.8	0.2	6.0	2.5	2.0
ThO <sub>2</sub>	0.1	0.1	0.1	0.1	0.9	0.7	1.4	0.1	3.3	1.4	2.6
TREO	0.8	0.4	0.8	0.4	0.7	0.3	1.5	0.2	1.3	0.3	1.4
BaO									0.5	0.3	0.3
F	3.4	0.6	4.2	0.1	4.0	0.1	3.5	0.1	1.4	0.6	2.7
Cl									0.1	0.1	0.1
-O=F <sub>2</sub>	1.4	0.3	1.8	0.0	1.7	0.1	1.5	0.1	0.6	0.3	1.1
Total	99.0	1.3	100.4	0.5	98.5	0.3	97.3	1.0	92.9	1.2	95.9
APFU <sup>1</sup>											
Nb <sub>2</sub> O <sub>5</sub>	1.872		1.908		1.810		1.689		1.445		1.624
Ta <sub>2</sub> O <sub>5</sub>	0.023		0.001		0.003		0.045		0.093		0.049
TiO <sub>2</sub>	0.094		0.081		0.153		0.178		0.245		0.193
ZrO <sub>2</sub>			0.004		0.020		0.073		0.090		0.065
SiO <sub>2</sub>	0.011		0.006		0.013		0.014		0.128		0.069
B-site	2.000		2.000		2.000		2.000		2.000		2.000
CaO	1.002		1.052		1.104		0.985		0.744		0.948
Na <sub>2</sub> O	0.577		0.771		0.707		0.547		0.115		0.382
FeO	0.042		0.013		0.008		0.018		0.169		0.082
SrO	0.047		0.034		0.019		0.023		0.084		0.053
UO <sub>2</sub>	0.014						0.010		0.088		0.029
ThO <sub>2</sub>	0.001		0.001		0.012		0.019		0.049		0.038
TREO	0.019		0.019		0.017		0.034		0.031		0.032
BaO									0.014		0.008
A-site	1.703		1.891		1.869		1.637		1.294		1.571
A vacancies	0.297		0.109		0.131		0.363		0.706		0.429
F	0.663		0.806		0.766		0.679		0.284		0.524
Cl									0.016		0.010
(OH,O,O <sub>2</sub> ,H	0.337		0.194		0.234		0.321		0.700		0.466

APFU<sup>1</sup> - atoms per formula unit. Calculated on a base that  $\sum B=2$ (OH,O,O<sub>2</sub>,H<sub>2</sub>O)<sup>2</sup> - Site Y, calculated as  $1-\sum(F,Cl)$ 

sd - standard deviation


empty cells - below the detection limit



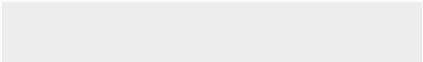

Carbonatite.

		Carbonatite		
Rim				
sd	22	sd	15	sd
4.6	65.3	1.3	66.8	3.2
1.5	0.3	0.2	0.6	1.1
0.4	3.5	0.3	2.1	0.8
1.3	1.0	0.8	0.5	1.1
0.9	0.2	0.2	0.3	0.3
2.2	16.5	0.5	14.6	1.0
1.4	5.9	0.3	6.3	1.1
0.9	0.1	0.1	0.2	0.3
0.9	0.5	0.1	1.4	0.6
1.9			0.1	0.2
0.8	1.6	0.6	1.0	1.6
0.3	1.1	0.3	1.2	0.7
0.4				
0.8	3.9	0.2	4.0	0.4
0.1				
0.4	1.7	0.1	1.7	0.2
1.9	98.4	0.4	97.4	1.1
1.795		1.864		
0.005		0.011		
0.162		0.096		
0.028		0.014		
0.010		0.016		
2.000		2.000		
1.077		0.968		
0.697		0.750		
0.007		0.011		
0.019		0.050		
		0.001		
0.023		0.014		
0.025		0.028		
1.849		1.822		
0.151		0.178		
0.757		0.785		
0.243		0.215		





Click here to access/download  
**Supplementary file**  
Table A1.xlsx



### Declaration of interests

- ☒ The authors declare that they have no known competing financial interests or personal relationships that could have appeared to influence the work reported in this paper.
- ☐ The authors declare the following financial interests/personal relationships which may be considered as potential competing interests: